Since January 2020 Elsevier has created a COVID-19 resource centre with free information in English and Mandarin on the novel coronavirus COVID-19. The COVID-19 resource centre is hosted on Elsevier Connect, the company's public news and information website.

Journal of Inorganic Biochemistry 234 (2022) 111899

Contents lists available at ScienceDirect

Journal of Inorganic Biochemistry

journal homepage: www.elsevier.com/locate/jinorgbio

Decavanadate interactions with the elements of the SARS-CoV-2 spike protein highlight the potential role of electrostatics in disrupting the infectivity cycle

Daniel Favre [a], Jackson F. Harmon [b], Ali Zhang [c], Matthew S. Miller [c], Igor A. Kaltashov [a,b,*]

[a] Department of Chemistry, University of Massachusetts-Amherst, Amherst, MA 01003, United States of America
[b] Institute for Applied Life Sciences, University of Massachusetts-Amherst, Amherst, MA 01003, United States of America
[c] Michael G. DeGroote Institute for Infectious Disease Research, McMaster Immunology Research Centre, Department of Biochemistry and Biomedical Sciences, McMaster University, Hamilton, ON L8S 4L8, Canada

ARTICLE INFO

Keywords:
Polyoxidometalate
Vanadium
Coronavirus
Therapeutics
Antiviral agent
Polyanion

ABSTRACT

Polyoxidometalates (POMs) exhibit a range of biological properties that can be exploited for a variety of therapeutic applications. However, their potential utility as antivirals has been largely overlooked in the ongoing efforts to identify safe, effective and robust therapeutic agents to combat COVID-19. We focus on decavanadate (V10), a paradigmatic member of the POM family, to highlight the utility of electrostatic forces as a means of disrupting molecular processes underlying the SARS-CoV-2 entry into the host cell. While the departure from the traditional lock-and-key approach to the rational drug design relies on less-specific and longer-range interactions, it may enhance the robustness of therapeutic agents by making them less sensitive to the viral mutations. Native mass spectrometry (MS) not only demonstrates the ability of V10 to associate with the receptor-binding domain of the SARS-CoV-2 spike protein, but also provides evidence that this association disrupts the protein binding to its host cell-surface receptor. Furthermore, V10 is also shown to be capable of binding to the polybasic furin cleavage site within the spike protein, which is likely to decrease the effectiveness of the proteolytic processing of the latter (a pre-requisite for the viral fusion with the host cell membrane). Although *in vitro* studies carried out with SARS-CoV-2 infected cells identify V10 cytotoxicity as a major factor limiting its utility as an antiviral agent, the collected data provide a compelling stimulus for continuing the search for effective, robust and safe therapeutics targeting the novel coronavirus among members of the POM family.

1. Introduction

Two years after being declared a pandemic by the World Health Organization, COVID-19 [1] shows no signs of abating, with the disease continuing to overwhelm healthcare systems worldwide, and the total number of fatalities already exceeding six million. The initial enthusiasm associated with the fast development and effective roll-out of the novel coronavirus vaccines [2–5] has tapered off following the realization that their protection is not absolute [6], and durability is limited [7], mirroring the rapid decay of immune protection against recurring SARS-CoV-2 infections in former COVID-19 patients [8]. The immune evasion problem has been exacerbated by the emergence and rapid proliferation of the novel variants of the SARS-CoV-2 in the second half of 2021, *viz.* Delta and Omicron [9]. The multiple mutations giving rise to each novel variant also reduce the effectiveness of monoclonal antibody (mAb) therapies [10], diminishing available treatment options. At the same time, certain trends that are beginning to emerge from the analyses of SARS-CoV-2 mutations suggest that there may be alternative ways to design effective antiviral therapies. For example, multiple studies highlighted the anomalously high incidence of mutations that convert acidic or neutral residues of the SARS-CoV-2 spike glycoprotein (S) to basic ones both within the receptor-binding domain (RBD) [11–13] and the furin cleavage site [14]. The latter (particularly P681R - incorporation of an additional arginine residue within the PRRAR segment) is advantageous from the point of view of the increased susceptibility of S to the proteolytic processing by the host enzymes critical for the viral particle's ability to fuse with the host cell membrane. At the same time, the increased density of basic residues within RBD enhances

* Corresponding author at: 240 Thatcher Road, Life Science Laboratories N369, University of Massachusetts-Amherst, Amherst, MA 01003, United States of America.
E-mail address: kaltashov@chem.umass.edu (I.A. Kaltashov).

https://doi.org/10.1016/j.jinorgbio.2022.111899
Received 23 March 2022; Received in revised form 2 June 2022; Accepted 5 June 2022
Available online 9 June 2022

docking of the viral particle to its host cell surface receptor angiotensin-converting enzyme 2 (ACE2) *via* electrostatic interactions with the low-pI ectodomain of this protein. This facilitates the initial anchoring of the virus in the extra-cellular matrix (ECM) by promoting stronger interactions with the polyanionic heparan sulfate chains of the proteoglycans, the major component of the ECM [13]. In fact, several studies have pointed out at the electrostatic potential changes within S as the major factor responsible for the higher transmission rates of both Delta and Omicron [11,12].

While the S mutations promoting a higher net positive charge within the key structural segments are advantageous vis-à-vis the ability of the virus to infect host cells, they also increase the pathogen's vulnerability to therapeutic agents that act by disrupting the electrostatic interactions. Indeed, several reports pointed out that a highly anionic polysaccharide heparin, as well as some of its derivatives, may be effective at inhibiting the host cell entry by the SARS-CoV-2 [15–17], and this polyanion has been already used in both treatment and prophylaxis of COVID-19 [18–21]. Although some of the therapeutic benefits of heparin in COVID-19 patients are due to its anticoagulant and anti-inflammatory properties, it is clear that its ability to interact with the key structural elements of SARS-CoV-2 S and block their association with the cell-surface receptors (such as the RBD/ACE2 binding [22]), also play an important role in mitigating the pathogenesis. Importantly, the long-range nature of the electrostatic interactions between polyanions (such as heparin) and S make them much less susceptible to the mutations within the latter. In fact, a range of mutations that gave rise to the Delta and Omicron (*vide supra*) would enhance the polyanion/S interactions, an effect that would be opposite to the antibody escape phenomenon that currently limits both the utility of mAb-based therapies and the extent of the acquired immune protection [9,23]. Unfortunately, broader utilization of heparin-like polyanions in the COVID-19 therapeutic practice raises serious concerns, as this century-old anticoagulant may induce internal bleeding in some patients, while triggering potentially deadly heparin-induced thrombocytopenia in others [24]. These considerations motivate the search for alternatives that will be able to interact effectively with the positively-charged segments of S *via* long-range electrostatic forces that are less sensitive to the viral mutations compared to the short-range lock-and-key type of interactions, while at the same time lacking the properties of heparin that reduce the attractiveness of this polysaccharide in the COVID-19 setting.

Polyoxidometalates (POMs) are a class of polynuclear inorganic compounds, which are mostly comprised of transition metal and oxygen atoms, although other atoms (such as phosphorus and silicon) may also be involved [25,26]. Many POMs are polyanions, a property that endows them with a range of diverse biological activities (many of which can be potentially exploited for therapeutic purposes) that are mostly mediated by electrostatic interactions [27,28]. In this work we explore the ability of decavanadate (V10, $V_{10}O_{28}^{6-}$), a paradigmatic member of the POM family, to interact with two positively charged structural segments of the SARS-CoV-2 S that play critical roles in the host cell infection (RBD and the furin cleavage site). We demonstrate that V10 not only interacts with both of these segments at physiological ionic strength, but in fact inhibits the RBD/ACE2 association, a key step in the cell infection process. Although V10 cannot be viewed as a viable antiviral agent due to its cytotoxic properties (as revealed by the *in vitro* studies with the SARS-CoV-2 infected cells presented in this work), its ability to interfere with the key processes underlying the infectivity of the novel coronavirus certainly warrants a more extensive search for novel and effective antivirals among other members of the POM family.

2. Experimental

2.1. Materials

The recombinant forms of the receptor binding domains of SARS-CoV-2 S-protein (RBD) expressed in the baculovirus system and the ectodomain of the human angiotensin-converting enzyme 2 (ACE2) were purchased form Sino Biologics (Wayne, PA). The purity of both proteins was examined by intact-mass MS measurements as described earlier [22]. The synthetic FCS model peptide (YQTQTNSPRRARSVAS, S residues 674–689, UniProt P0DTC2) was purchased from Biomatic (Cambridge, ON, Canada). The identity and purity of the synthetic peptide were verified by LC/MS/MS. All protein and peptide solutions were prepared in 150 mM ammonium acetate, pH adjusted to 7. Throughout all measurements, protein solutions were maintained at physiological ionic strength (150 mM ammonium acetate) to eliminate potential artifacts due to electrostatic interactions. V10 was synthesized as ammonium decavanadate salt by dissolving 2.997 g of ammonium metavanadate (Sigma-Aldrich, St. Louis, MO) in 100 mL of deionized water and titrating the resulting solution to pH 4 with formic acid and filtering the resulting solution. $(NH_4)_6V_{10}O_{28}$ was then precipitated by the addition of 150 mL of 95% ethanol and subsequently collected and washed *via* vacuum filtration. The product's identity and purity were verified using mass spectrometry as described earlier [29]. ESI MS was also used to verify the kinetic stability of V10 in aqueous solutions at pH 7 and relevant concentration (1–10 μM) for the time periods required for measuring V10/protein and V10/peptide interaction.

2.2. Mass Spectrometry

MS characterization of RBD and RBD/V10 interactions was carried out using a Synapt G2S (Waters, Milford, MA) hybrid quadrupole/time-of-flight mass spectrometer equipped with a nanospray source. Typical instrument parameters for native MS analysis were as follows: capillary, 1.3 kV; source temperature, 20 °C; sampling cone, 120.00 V; extraction cone, 5.00 V; nanoflow gas pressure, 0.30 Bar. The mass calibration was carried out externally using perfluoroheptanoic acid. Processing of the raw MS data was carried out using the UniDEC deconvolution algorithm [30], with the charge state assignment assisted by the limited charge reduction [31]. Isolation of ionic populations in the trap cell for limited charge reduction measurements was performed by setting the quadrupole LM resolution values in the range of 4.3–4.7; and the gas phase polycation/anion reaction were triggered by introducing 1,3-dicyanobenzene anions after setting the trap wave height to 0.4–1.5 V. The anions were produced in the API source by setting the discharge current at 20 μA. Data fitting was performed with R-Studio using nonlinear least-squares fit with a convolution of Gaussian peaks (*dnorm*).

MS characterization of the FCS peptide and its interactions with V10 was carried out with a Solarix 7 (Bruker Daltonics, Billerica, MA) Fourier-transform ion cyclotron resonance (FT ICR) mass spectrometer equipped with a conventional ESI source and a 7 T superconducting magnet. All measurements were carried out in the positive ion mode using the following instrument parameters: ESI capillary, 4000 V; end plate offset, −500 V; nebulizer, 1.6 bar; dry gas, 4.0 L/min; dry temperature, 150 °C; capillary exit, 190 V; deflector plate, 190 V; funnel 1, 150 V, skimmer 1, 15 V; funnel RF amplitude, 200 V_{p-p}. The mass calibration was carried out externally using sodium formate as a calibrant.

2.3. In vitro studies of V10 cytotoxicity and anti-viral properties

Vero E6 (ATCC CRL-1586) or U87mg-hACE2 cells were seeded in opaque 96 well flat-bottom plates (Costar) in complete DMEM (supplemented with 10% FBS, 1% L-glutamine, 100 U/mL penicillin-streptomycin, and 50 mg/mL Geneticin for hACE2 cells). The media was replaced 24 h post-seeding with complete DMEM containing indicated concentrations of V10 or solvent. 24 h after pre-treatment, the media was replaced with SARS-CoV-2/SB3-TYAGNC [32] at a multiplicity of infection of 0.01, equalling to 300 PFU/well with indicated concentrations of V10 or solvent diluted in low serum DMEM (supplemented with 2% FBS, 1% L-glutamine, 100 U/mL penicillin-streptomycin). The cells were then incubated at 37 °C for 3 days (Vero

E6 and U87mg-hACE2) before cell viability was determined. The plates were read by removing 50 μL of culture supernatant and adding 50 μL of CellTiter-Glo 2.0 Reagent (Promega) to each well. The plates were then shaken for 2 min, followed by reading the luminescence using a BioTek Synergy H1 or SpectraMax i3 microplate reader with gain of 135 and integration time of 1 s.

3. Results

3.1. V10 interaction with RBD

Consistent with the previous reports [22], native MS analysis of RBD reveals a broad distribution of ionic signal featuring a significant overlap of ions corresponding to different charge states (Fig. 1). Straightforward application of deconvolution algorithms to process MS data for such heterogeneous systems usually fails [33], and the charge state assignment was carried out by selecting ionic populations within narrow *m/z* windows followed by their brief exposure to radical anions. This process (known as limited charge reduction) allows well-defined charge ladders to be obtained, from which both ionic charges and masses can be readily calculated [31]. Application of this technique to the mass spectrum of RBD reveals the presence of both the monomeric form of RBD (ionic signal within the *m/z* range 2500-3500; the average mass of 32.3 kDa) and a less abundant dimeric form of the protein in the *m/z* region above 3500. The latter most likely arises due to formation of an external disulfide bond that involves a single unpaired cysteine residue within the RBD construct, as has been reported earlier [22]. Addition of a nearly stoichiometric amount of V10 to the protein solution results in a noticeable change of the appearance of the mass spectrum (compare the blue and red traces in the Fig. 1 inset). The convoluted appearance of this mass spectrum prevented application of common deconvolution procedures as a means of extracting mass distributions from the raw MS data (as was the case with free RBD – *vide supra*). However, the presence of inflection points within spectral features representing unique charge states indicates that at least two components contribute to the overall ionic signal (*e.g.*, the ligand-free and ligand-bound forms of the protein). In order to verify that the latter is indeed an RBD·V10 complex, the ionic signal of RBD was modeled as a sum of normally distributed signals for all detected charge states:

$$S_{total}^{RBD}(\mu) = \sum A_z^{RBD} \bullet e^{-\frac{(z+\mu z-M_O)^2}{2\sigma^2}}, \quad (1)$$

where A_z is the signal amplitude for the charge state z; M_O and σ are the average and the standard deviation of the protein mass distribution; and μ is the numeric m/z value. The best fit was obtained by carrying out the minimization routine to optimize the values of σ and A_z (for $z = 10$–13). The lower charge states were excluded, since the corresponding ionic signals overlap with that of the dimeric form of the protein (*vide supra*). The results are presented in Fig. 1 (bottom), with all charge states shown individually. Processing the mass spectrum of RBD acquired in the presence of V10 was carried out by assuming that the ionic signal representing the RBD·V10 complex is also distributed normally, and the standard deviation of this distribution is the same as for RBD alone:

$$S_{total}(\mu) = \sum \left(A_z^{RBD} \bullet e^{-\frac{(z+\mu z-M_O)^2}{2\sigma^2}} + A_z^{RBD \bullet V10} \bullet e^{-\frac{(z+\mu z-(M_O+M_{V10}))^2}{2\sigma^2}} \right), \quad (2)$$

where M_{V10} is the average mass of the electrically neutral form of V10, $H_6V_{10}O_{28}$ (963.4 Da). The data fitting results for the MS data acquired for RBD in the presence of V10 are presented in Fig. 1 (top), with the simulated signals representing RBD alone and in complex with V10 shown in blue and red, respectively. The quality of the data fits can be further improved by modifying the intensity distributions for each charge state to account for the asymmetry (peak tailing towards higher *m/z* values due to the incomplete desolvation of protein ions in the ESI interface). However, the extent of residual solvation depends on the charge state *z*, and the mathematical expressions for the ionic signal will include a significantly larger number of variable parameters compared to (1) and (2). As a result, nearly-perfect fits can be readily obtained using different sets of optimized parameters (*i.e.*, in this case there is no unique solution to the optimization problem). Therefore, we restricted our calculations to the limited set of variable parameters, and the results are consistent with the notion of RBD interacting with V10 in solution giving rise to complexes of 1:1 protein:POM stoichiometry. Furthermore, the absence of the ionic signal corresponding to the complexes of higher stoichiometry indicates that the RBD/V10 interaction is specific, as opposed to being a result of the non-specific adduct formation process occurring in the ESI interface.

The influence of V10 binding to RBD on the ability of the latter to

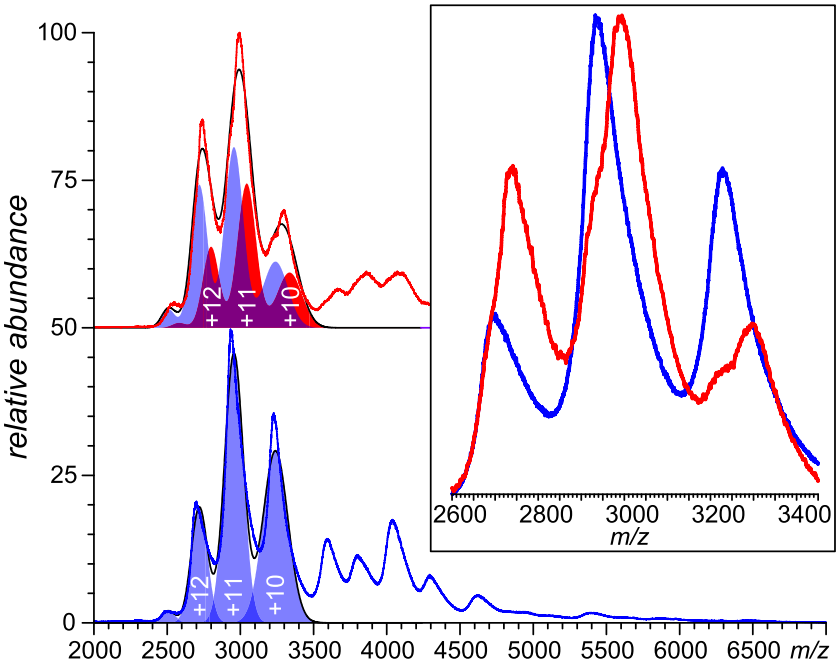

Fig. 1. Mass spectra of 6 μM RBD solutions in 150 mM ammonium acetate acquired in the presence of 5 μM V10 (red traces) and in the absence of the polyanion (blue traces). Each mass spectrum is normalized to the highest intensity peak. The inset shows an overlay of the two spectra in the RBD monomer region. The colour-filled curves represent the best-fit charge state distributions constructed for the RBD and RBD·V10 ions assuming normal intensity distribution for each charge state (the *m/z* region above 3500 was not used for fitting, as it contains contributions from both monomeric and dimeric forms of RBD). (For interpretation of the references to colour in this figure legend, the reader is referred to the web version of this article.)

associate with the SARS-CoV-2 host cell-surface receptor, ACE2, was studied by acquiring native mass spectra of an aqueous solution of a mixture of RBD (2.9 μM) and the recombinant form of the ectodomain of human ACE2 (1.9 μM) at physiological pH/ionic strength both in the presence and in the absence of V10. The RBD/ACE2 mass spectrum features an abundant signal within the *m/z* range 6500–8000 with partially resolved charge states (Fig. 2A). Fitting this distribution using an approach similar to that outlined above (*i.e.*, using eq. (1), *mutatis mutandis*) without fixing the M_O value gives rise to a range of charge states (see the purple colour-filled curves in Fig. 2A) and the average mass value of 248.3 kDa, consistent with the previously reported mass of the RBD_2ACE2_2 complex [22] (since the ectodomain of ACE2 forms a stable dimer under near-native conditions, which can partially dissociate under certain conditions, we will use the $ACE2_2$ notation to designate the canonical dimeric form of this protein in order to avoid confusion). Addition of V10 to the RBD/ACE2 mixture (to a final concentration of 5 μM) results in a noticeable change of the appearance of the mass spectrum in the high *m/z* region (Fig. 2B). The ionic signal shifts to a slightly lower *m/z* region (6000-7000), and processing this signal using the data fitting procedure outlined above yields notably lower values of the charge states and the average mass (184.0 kDa), consistent with the mass of $ACE2_2$ free of RBD. Importantly, no signal corresponding to a putative partially saturated $RBD{\cdot}ACE2_2$ complex could be detected, consistent with the notion of a complete dissociation of RBD from ACE2.

3.2. V10 interaction with furin cleavage site model peptide (ESI MS)

Evaluation of V10 interaction with the furin cleavage site of S was carried out using a peptide YQTQTNSPRRARSVAS (S residues 674–689, UniProt P0DTC2), which incorporates the arginine-rich segment recognized by serine proteases. The high-resolution mass spectrum of this peptide (labeled FCS in Fig. 3) undergoes a notable change upon addition of a small molar excess of V10 to the peptide solution. In addition to peaks representing the unbound forms of the peptide (charge states +2 and + 3) and V10 ($H_7V_{10}O_{28}^+$ and $NH_4H_6V_{10}O_{28}^+$, the positive charge states of which are expected and consistent with the previous work [29]), a prominent signal is observed at *m/z* 929. The experimentally measured monoisotopic *m/z* value for this ion is 929.0908, a number that is within 7 ppm of the calculated monoisotopic *m/z* value for the +3 charge state of the FCS·V10 complex ion (929.0967). These measurements were carried out at physiological ionic strength to eliminate non-specific electrostatic interaction in solution. In addition to the +3 charge state of the FCS·V10 complex, a weaker ion signal was detected for the +2 charge state (the measured monoisotopic *m/z* value 1393.1311 *vs.* the calculated one of 1393.1414). Minor signals were also

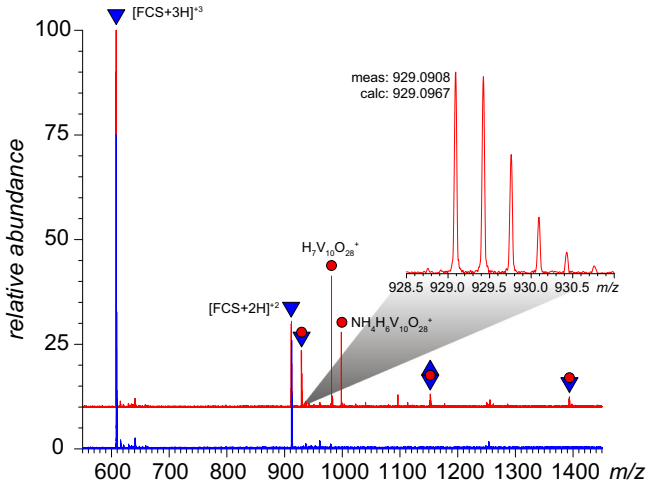

Fig. 3. Mass spectra of the FCS model peptide (10.0 μM) and FCS/V10 mixture (10.0/10.25 μM) in 150 mM ammonium acetate (blue and red traces, respectively). The inset shows isotopic distribution of ions representing the FCS·V10 complex. (For interpretation of the references to colour in this figure legend, the reader is referred to the web version of this article.)

detected for the $FCS_2{\cdot}V10$ (charge state +4, monoisotopic *m/z* 1152.3001) and $FCS{\cdot}V10_2$ complexes (charge state +3, monoisotopic *m/z* 1255.8000). Increasing the concentration of V10 in solution (up to a 5-fold molar excess over the model peptide) resulted in an increase of the relative abundance of ions representing the FCS·V10 complex, but ions corresponding to the free peptide were always present in the mass spectra (data not shown).

3.3. In vitro evaluation of V10 antiviral properties and cytotoxicity

Evaluation of the anti-viral activity of V10 was carried out using both human U87mg-hACE2 and Vero E6 cells. The cells were challenged with SARS-CoV-2 (300 PFU/well), resulting in a significant decrease of their viability (Fig. 4). Addition of V10 to the infected cell cultures did not result in any noticeable increase of the cell viability at levels as high as 1 μM. In human cells, a transient viability increase was observed above 1 μM, but was immediately followed by a precipitous decline (Fig. 4A). This dramatic decrease in the cell viability at 10 μM and above mirrored behavior of the uninfected cells, which clearly manifested V10 cytotoxicity in that concentration range. The cytotoxicity could be clearly ascribed to V10, rather than other components of the mildly acidic V10

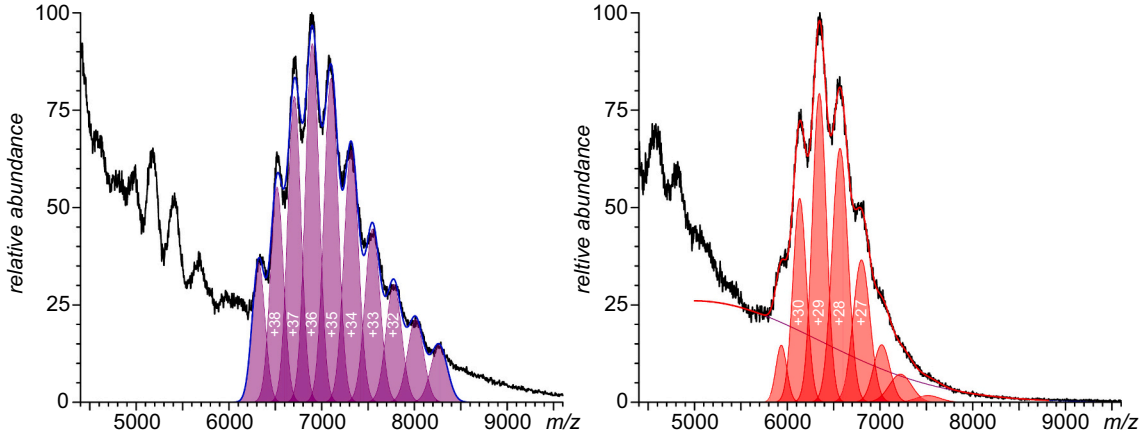

Fig. 2. Native MS of the RBD/ACE2 mixture (2.9 and 1.9 μM, respectively, in 150 mM ammonium acetate) in the absence (A) and in the presence of 5.0 μM V10 (B). The sigmoidal curve shows a simulated background signal.

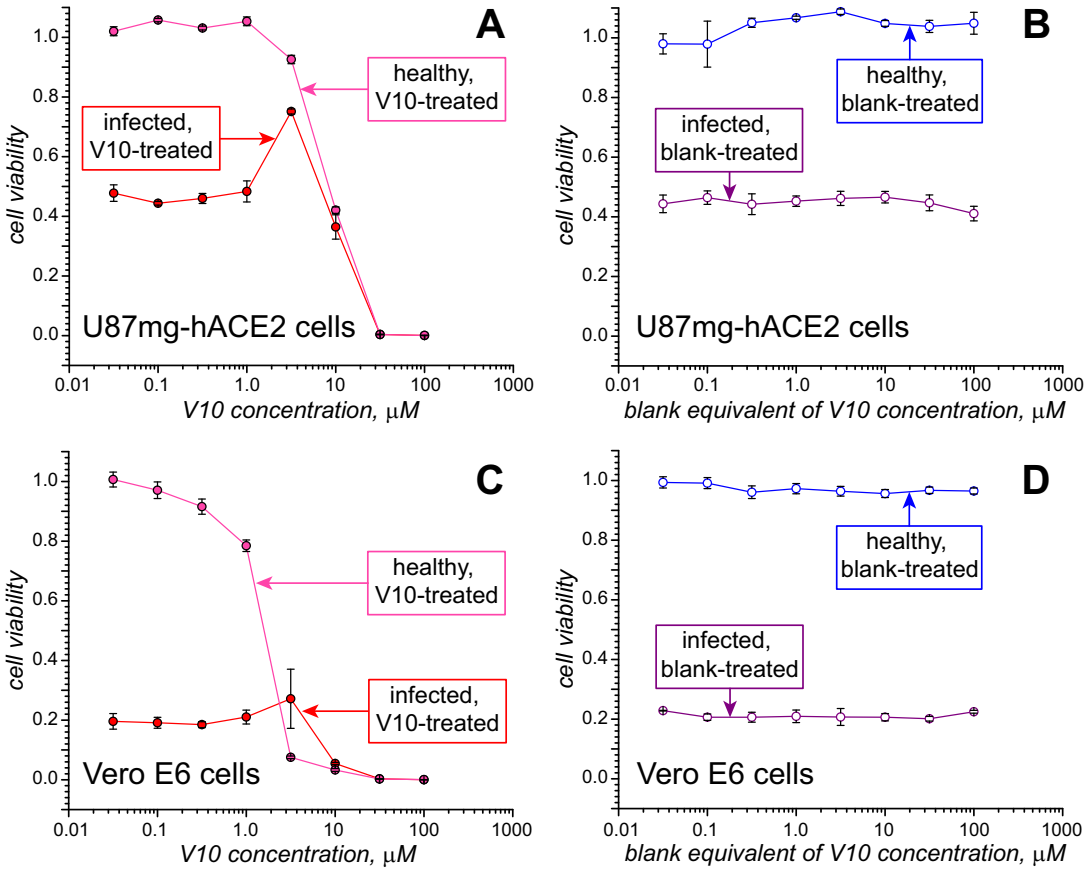

Fig. 4. Viability of U87mg-hACE2 (A) and Vero E6 (C) cells infected with SARS-CoV-2 in the presence of varying concentrations of V10 (red) compared to the viability of uninfected cells in the presence of V10 (magenta). Diagrams on the right show the viability of U87mg-hACE2 (B) and Vero E6 (D) cells infected with the virus (purple) in the presence of varying concentrations of the solvent components of the V10 sample used for experiments shown in the left panel. The blue dots show the same measurements for healthy (uninfected) cells. (For interpretation of the references to colour in this figure legend, the reader is referred to the web version of this article.)

solution used in these measurements, as no change in the cell viability was detected when both virus-challenged and healthy (uninfected) cells were treated with the equivalent amounts of the "blank" (a solution having identical composition to the V10 stock solution, but lacking the inorganic polyanion), as shown in Fig. 4B. The Vero cells also exhibited remarkable susceptibility to V10 at doses exceeding 10 μM (Fig. 4C), while remaining insensitive to other components of the V10 solution (Fig. 4D).

4. Discussion

The major route of the SARS-CoV-2 entry into the host cell (Fig. 5) exploits the ability of S [34] to associate with ACE2 [35], which is ubiquitously expressed on the surface of many cell types. The electrostatic forces not only play an important role in the interaction between the RBD of the SARS-CoV-2 S with ACE2 (which has a theoretical pI of 5.36) [36], but also in the initial encounter of the virus with the host cell, which is mediated by the heparan sulfate (HS) proteoglycans [37]. The critical dependence of the viral docking on the electrostatic interactions

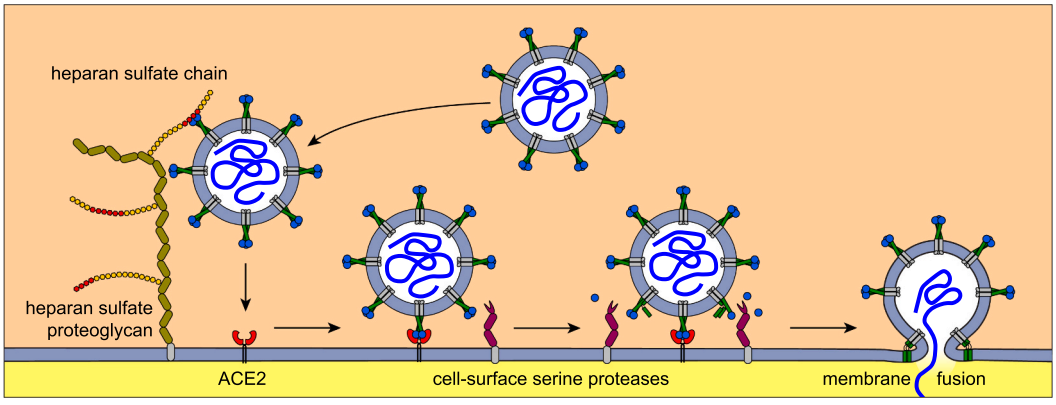

Fig. 5. A schematic diagram of the key steps of SARS-CoV-2 entry into the host cell *via* ACE-2 mediated (non-endosomal) pathway.

suggests that it can be potentially exploited for therapeutic purposes. In fact, the success of the polyanionic biopolymer heparin and heparin-derived medicines in mitigating the pathological consequences of COVID-19 infection [19,20] is attributable, at least to some extent, to their ability to associate with RBD and prevent its interaction with both HS proteolglycans and ACE2 [15,22,38,39]. Native MS (Fig. 1) provides convincing evidence that V10 has the ability to associate with RBD in solution under physiologically relevant conditions (neutral pH and physiological ionic strength), which is not surprising given its polyanionic nature. However, the ability of V10 to associate with RBD does not necessarily mean that it would diminish the affinity of the latter for the cell-surface receptor. Indeed, there are two well-defined and extended positive-charge patches on the surface of RBD (Fig. 6), where V10 binding can occur due to significant electrostatic attraction, but only one of them has a significant overlap with the receptor-binding motif. Nevertheless, the native MS characterization of the RBD/ACE2 interaction clearly indicates that the presence of V10 in solution results in a facile disassembly of the RBD/ACE2 complex (Fig. 2). This behavior mirrors the effect of short heparinoids (such as the highly anionic pentasaccharide fondaparinux) on RBD, which form only 1:1 complexes with the protein but nonetheless effectively disrupt its interaction with the receptor [22,40]. Interestingly, the results of the earlier molecular modeling work in the case of RBD/short heparinoid association suggest that the polyanion binding to the protein occurs outside of its receptor-binding motif; nonetheless, the ensuing conformational changes rearrange the latter allosterically to an extent that is sufficient to disrupt the RBD/ACE2 interaction [22]. It is possible that the V10 interference in the RBD/ACE2 interaction follows a similar scenario, although native MS alone obviously cannot provide atomistic details of this process. What is clear is the fact that this interference is sufficiently effective, highlighting the potential of V10 to act as a disruptor of the virus docking to the cell surface, although it is important to remember that the avidity of the S/ACE2 interactions (*i.e.*, binding of a single virion particle to multiple receptors on the cell surface) could influence the efficacy of V10 differentially in an infection model relative and an *in vitro* binding assay.

Another critical step in the viral cell entry that can be potentially inhibited by electrostatic interactions is the proteolytic processing of S by the cell-surface proteases. This makes its fusion peptide (localized in the S2 domain of the protein close to the segment connecting the S1 and S2 domains) available for anchoring into the cell membrane, which is followed by fusion of the virus with the cell [41], a mechanism common to all coronaviruses [42] (Fig. 5). The two main actors (furin and the transmembrane serine protease 2, or TMPRSS2) recognize two distinct sites within the segment connecting its S1 and S2 domains [14]. While the activation of S fusogenic activity is performed by TMPRSS2 (which cleaves the SGP polypeptide chain at the so-called S2' cleavage site on the N-terminal side of the fusion peptide) [14], this step cannot be completed without the S priming by furin. The latter processes the S polypeptide chain at the so-called S1/S2 cleavage site, which incorporates the polybasic RRAR furin recognition element [43]. Although furin is a part of the host cell secretory machinery [44,45], and is believed to process the nascent S chains generated inside the cell upon the virus' hijacking the cellular protein expression system [46], it can also be present on the cell surface and even released into circulation [47]. In fact, the presence of furin on the cell surface is required for toxin activation and cell entry by a range of bacterial pathogens [48,49]. Therefore, it is reasonable to assume that at least a fraction of the SARS-CoV-2 S are processed by furin either on the cell surface or while in circulation. Furthermore, several other blood-borne serine proteases, such as factor Xa and thrombin, can also process S, enhancing the viral cell entry and exacerbating infectivity [50].

The polybasic furin cleavage site located within S has anomalous degree of conformational motility as predicted by multiple algorithms comprising the PONDR (Predictor of Natural Disordered Regions) engine [51] (nor is this segment visible in the crystal structures of this protein [34,52,53]). Therefore, a polypeptide with an amino acid sequence corresponding to this unstructured region can be used as a realistic model of this S segment (residues 674–689, YQTQTNSPRRARSVAS, which we refer to as FCS). The arginine-rich part of this sequence endows FCS with a significant positive charge, which had been shown to have affinity to anionic biopolymers, such as heparin [39]. The polyanionic nature of V10 suggests that it may also interact with the arginine-rich segment of the FCS, and the mass spectrum of this peptide acquired in the presence of V10 (Fig. 3) indicates that the two oppositely charged molecules do form a complex in solution despite the charge-screening effect of the salt. It remains to be seen to what extent the proteolytic processing of FCS is inhibited by this interaction; nevertheless, it seems plausible that binding of a bulky inorganic molecule, such as V10, to the protease substrate right at the cleavage site would interfere with the proteolysis. At the same time, we note that the presence of the abundant signals of the free peptide and V10 alongside the FCS·V10 complexes in the mass spectrum shown in Fig. 3 indicates that the interaction is not very strong. Although no affinity measurements were performed in this work, an estimate based on the total FCS and V10 concentrations, as well as the relative intensities of the signal [54] suggest that the K_D value for this system exceeds the 10^{-5} M level. Although this represents transient interaction within the peptide/POM system, it may interfere with the enzymatic processing of the furin cleavage side given sufficient concentrations of the polyanionic ligand.

The results of the experimental work discussed so far provide a clear indication that V10 has a capability to interfere with the key steps of the SARS-CoV-2 infectivity cycle. While the conclusions of the studies carried out with the model proteins and peptides are encouraging, they do not provide evidence that SARS-CoV-2 entry can be inhibited in living cells using the physiologically reasonable (safe) concentrations of the

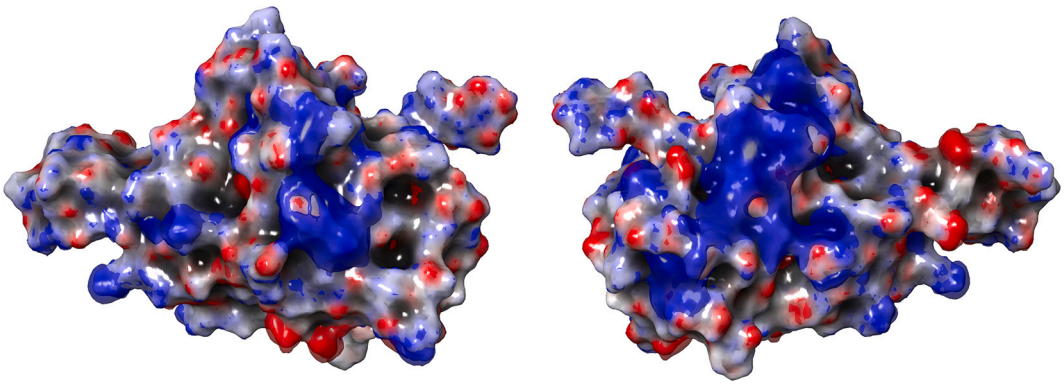

Fig. 6. Electrostatic potential ($3kT/e$) surfaces of RBD shown from the ACE2-binding side (left) and the opposite side (right) based on the crystal structure from PDB 6M17. Each of the two extended positive-charge basins can serve as a binding site for the polyanionic V10 under physiological conditions.

inhibitor. The latter can be verified only using *in vitro* models, and unfortunately the cell culture work indicates that V10 is cytotoxic at concentration levels above 1 μM (Fig. 4). Interestingly, these studies also indicate that V10 may begin to manifest its antiviral properties right before the onset of the cytotoxicity. Although one might see the results of the *in vitro* work presented in Fig. 4 as disappointing, as V10 fails to effectively inhibit viral infectivity at safe (sub-cytotoxic) levels, further work targeting regions of SARS-CoV-2 S protein vulnerability with inorganic polyanions is certainly warranted. Our work demonstrates that electrostatic forces can be exploited to interfere with the interactions between the virus and its physiological targets, and the enormous chemical and structural diversity exhibited by POMs [55] remains an untapped source of potential antivirals. Indeed, the therapeutic potential of this class of inorganic molecules is actively explored in areas ranging from oncology [56] to antibiotics [57], while their antiviral activity [58] received relatively little attention. While our work focused on the ability of one specific vanadium-based POM (V10) to target the key steps of the SARS-CoV-2 entry into the host cell (Fig. 5), vanadium exhibits a range of other biological activities, such as anti-inflammatory and anti-hyperglycemic effects, that are also beneficial vis-à-vis mitigating clinical manifestations of severe COVID-19 [59].

5. Conclusions

The relentless search for the effective and safe therapeutic treatments of COVID-19 continues to suffer setbacks due to the rapid evolution SARS-CoV-2. While the antiviral agents designed using the traditional lock-and-key approach [60] may be rendered ineffective by a single mutation, exploitation of the less specific/longer-range electrostatic interactions as an alternative therapeutic strategy may prove more robust. Heparin and related highly anionic polysaccharides had been actively investigated in this regard since the beginning of the pandemic [61,62], and have already entered clinical practice [20] despite some documented shortcomings [63]. At the same time, several other classes of electron-rich compounds remain largely overlooked, including inorganic polyanions such as POMs. Investigation of V10, a paradigmatic member of this family, vis-à-vis it ability to interfere with the key steps of SARS-CoV-2 entry into the host cell highlights the potential of POMs as effective disruptors of both the viral particle docking to the cell surface receptor (ACE2) and the following proteolytic processing required for activation of the fusogenic properties of the virus. Although the *in vitro* studies identify the cytotoxicity of V10 as a major factor limiting its utility as an antiviral agent, the collected data provide compelling evidence that the search for safe, effective and robust COVID-19 therapeutics among the members of the POM family is warranted.

Author contributions

I.K. and D.F. designed the study; D.F. produced the materials (V10); D.F. and J.H. carried out the MS-based experimental work; D.F., J.H. and I.K. processed and interpreted the MS data; A.Z. and M. M. designed and carried out the *in vitro* studies of the V10 influence on the SARS-CoV-2 infectivity. D.F. and I.K. wrote the manuscript. All authors participated in editing the manuscript and gave their consent to its final (submitted) version.

Declaration of Competing Interest

The authors declare that they have no known competing financial interests or personal relationships that could have appeared to influence the work reported in this paper.

Igor A. Kaltashov reports financial support was provided by the National Institutes of Health. Matthew Miller reports a relationship with the Ontario Research Fund that includes: funding grants.

Data availability

Data will be made available on request.

Acknowledgements

This work was supported by a grant R01 GM112666 from the National Institutes of Health. M.S.M. was supported, in part, by an Early Researcher Award from the Ontario Research Fund, and a Canada Research Chair (Tier 2) in Viral Pandemics. A.Z was supported by a Physician Services Incorporated Research Trainee Fellowship and a CHIR Canada Graduate Scholarships – Doctoral Award. All MS measurements were carried out in the Mass Spectrometry Core facility at UMass-Amherst. All work with SARS-CoV-2 was carried out in the McMaster University containment level 3 laboratory in accordance with all applicable biosafety regulations. The authors are grateful to Yi Du (UMass-Amherst) for help with preparing the figure illustrating the electrostatic potential surface of RBD.

References

[1] E. Estrada, COVID-19 and SARS-CoV-2. Modeling the present, looking at the future, Phys. Rep. 869 (2020) 1–51, https://doi.org/10.1016/j.physrep.2020.07.005.
[2] D.Y. Logunov, et al., Safety and immunogenicity of an rAd26 and rAd5 vector-based heterologous prime-boost COVID-19 vaccine in two formulations: two open, non-randomised phase 1/2 studies from Russia, Lancet 396 (2020) 887–897, https://doi.org/10.1016/S0140-6736(20)31866-3.
[3] L.A. Jackson, et al., An mRNA vaccine against SARS-CoV-2 - preliminary report, N. Engl. J. Med. 383 (2020) 1920–1931, https://doi.org/10.1056/NEJMoa2022483.
[4] P.M. Folegatti, et al., Safety and immunogenicity of the ChAdOx1 nCoV-19 vaccine against SARS-CoV-2: a preliminary report of a phase 1/2, single-blind, randomised controlled trial, Lancet 396 (2020) 467–478, https://doi.org/10.1016/s0140-6736(20)31604-4.
[5] F.P. Polack, et al., Safety and efficacy of the BNT162b2 mRNA Covid-19 vaccine, N. Engl. J. Med. 383 (2020) 2603–2615, https://doi.org/10.1056/NEJMoa2034577.
[6] M. Bergwerk, et al., Covid-19 breakthrough infections in vaccinated health care workers, N. Engl. J. Med. (2021), https://doi.org/10.1056/NEJMoa2109072 (in press).
[7] M. Shrotri, et al., Spike-antibody waning after second dose of BNT162b2 or ChAdOx1, Lancet (2021), https://doi.org/10.1016/s0140-6736(21)01642-1 in press (doi: 10.1016/s0140-6736(21)01642-1).
[8] F.J. Ibarrondo, et al., Rapid decay of anti–SARS-CoV-2 antibodies in persons with mild Covid-19, New Engl. J. Med. (2020), https://doi.org/10.1056/NEJMc2025179 (in press).
[9] D. Planas, et al., Considerable escape of SARS-CoV-2 omicron to antibody neutralization, Nature (2021), https://doi.org/10.1038/s41586-021-04389-z (in press).
[10] J. Chen, K. Gao, R. Wang, G.W. Wei, Revealing the threat of emerging SARS-CoV-2 mutations to antibody therapies, J. Mol. Biol. 433 (2021), 167155, https://doi.org/10.1016/j.jmb.2021.167155.
[11] S. Pascarella, et al., SARS-CoV-2 B.1.617 Indian variants: are electrostatic potential changes responsible for a higher transmission rate? J. Med. Virol. 93 (2021) 6551–6556, https://doi.org/10.1002/jmv.27210.
[12] S. Pascarella, et al., The electrostatic potential of the omicron variant spike is higher than in Delta and Delta-plus variants: a hint to higher transmissibility? J. Med. Virol. (2021) https://doi.org/10.1002/jmv.27528 (in press).
[13] C. Nie, et al., Charge matters: mutations in omicron variant favor binding to cells, Chembiochem: a Eur. J. Chem. Biol. (2022), https://doi.org/10.1002/cbic.202100681 (in press).
[14] M. Takeda, Proteolytic activation of SARS-CoV-2 spike protein, Microbiol. Immunol. 66 (2022) 15–23, https://doi.org/10.1111/1348-0421.12945.
[15] R. Tandon, et al., Effective inhibition of SARS-CoV-2 entry by heparin and enoxaparin derivatives, J. Virol. 95 (2021), https://doi.org/10.1128/jvi.01987-20.
[16] J.A. Tree, et al., Unfractionated heparin inhibits live wild type SARS-CoV-2 cell infectivity at therapeutically relevant concentrations, Br. J. Pharmacol. 178 (2021) 626–635, https://doi.org/10.1111/bph.15304.
[17] L.J. Partridge, et al., ACE2-independent interaction of SARS-CoV-2 spike protein with human epithelial cells is inhibited by unfractionated heparin, Cells 10 (2021), https://doi.org/10.3390/cells10061419.
[18] J. Liu, J. Li, K. Arnold, R. Pawlinski, N.S. Key, Using heparin molecules to manage COVID-2019, Res. Pract. Thromb. Haemost. 4 (2020) 518–523, https://doi.org/10.1002/rth2.12353.
[19] P. Viale, M. Bartoletti, Clinical experience with therapeutic dose of low-molecular-weight heparin, Infez. Med. 28 (2020) 118–121.
[20] J.A. Hippensteel, W.B. LaRiviere, J.F. Colbert, C.J. Langouët-Astrié, E.P. Schmidt, Heparin as a therapy for COVID-19: current evidence and future possibilities, Am. J. Phys. Lung Cell. Mol. Phys. 319 (2020) L211–L217, https://doi.org/10.1152/ajplung.00199.2020.

[21] G. Di Perri, The rationale for low-molecular weight heparin (LMWH) use in SARS-CoV-2 infection, Infez. Med. 28 (2020) 52–56.
[22] Y. Yang, Y. Du, I.A. Kaltashov, The utility of native MS for understanding the mechanism of action of repurposed therapeutics in COVID-19: heparin as a disruptor of the SARS-CoV-2 interaction with its host cell receptor, Anal. Chem. 92 (2020) 10930–10934, https://doi.org/10.1021/acs.analchem.0c02449.
[23] R.T. Eguia, et al., A human coronavirus evolves antigenically to escape antibody immunity, PLoS Pathog. 17 (2021), e1009453, https://doi.org/10.1371/journal.ppat.1009453.
[24] P. Lingamaneni, S. Gonakoti, K. Moturi, I. Vohra, M. Zia, Heparin-induced thrombocytopenia in COVID-19, J. Investig. Med. High Impact. Case Rep. 8 (2020), 2324709620944091, https://doi.org/10.1177/2324709620944091.
[25] D.-L. Long, E. Burkholder, L. Cronin, Polyoxometalate clusters, nanostructures and materials: from self assembly to designer materials and devices, Chem. Soc. Rev. 36 (2007) 105–121, https://doi.org/10.1039/b502666k.
[26] A. Müller, F. Peters, M.T. Pope, D. Gatteschi, Polyoxometalates: very large clusters-nanoscale magnets, Chem. Rev. 98 (1998) 239–272, https://doi.org/10.1021/cr9603946.
[27] J.C. Pessoa, et al., Binding of vanadium ions and complexes to proteins and enzymes in aqueous solution, Coord. Chem. Rev. 449 (2021) 39, https://doi.org/10.1016/j.ccr.2021.214192.
[28] M. Aureliano, et al., Polyoxidovanadates' interactions with proteins: an overview, Coord. Chem. Rev. 454 (2022), 214344, https://doi.org/10.1016/j.ccr.2021.214344.
[29] D. Favre, et al., Solution- and gas-phase behavior of decavanadate: implications for mass spectrometric analysis of redox-active polyoxidometalates, Inorg. Chem. Front. 9 (2022) 1556–1564, https://doi.org/10.1039/D1QI01618K.
[30] M.T. Marty, et al., Bayesian deconvolution of mass and ion mobility spectra: from binary interactions to polydisperse ensembles, Anal. Chem. 87 (2015) 4370–4376, https://doi.org/10.1021/acs.analchem.5b00140.
[31] R.R. Abzalimov, I.A. Kaltashov, Electrospray ionization mass spectrometry of highly heterogeneous protein systems: protein ion charge state assignment via incomplete charge reduction, Anal. Chem. 82 (2010) 7523–7526, https://doi.org/10.1021/ac101848z.
[32] A. Banerjee, et al., Isolation, sequence, infectivity, and replication kinetics of severe acute respiratory syndrome coronavirus 2, Emerg. Infect. Dis. 26 (2020) 2054–2063, https://doi.org/10.3201/eid2609.201495.
[33] C.E. Bobst, J. Sperry, O.V. Friese, I.A. Kaltashov, Simultaneous evaluation of a vaccine component microheterogeneity and conformational integrity using native mass spectrometry and limited charge reduction, J. Am. Soc. Mass Spectrom. 32 (2021) 1631–1637, https://doi.org/10.1021/jasms.1c00091.
[34] A.C. Walls, et al., Structure, function, and antigenicity of the SARS-CoV-2 spike glycoprotein, Cell 181 (2020) 281–292, https://doi.org/10.1016/j.cell.2020.02.058.
[35] Y. Wan, J. Shang, R. Graham, R.S. Baric, F. Li, Receptor recognition by the novel coronavirus from Wuhan: an analysis based on decade-Long structural studies of SARS coronavirus, J. Virol. 94 (2020), https://doi.org/10.1128/jvi.00127-20 e00127–00120.
[36] ACE2 Protein Overview: Sequence, Structure, Function and Protein Interaction. https://www.sinobiological.com/resource/ace2/proteins>, 2022.
[37] M. Bermejo-Jambrina, et al., Infection and transmission of SARS-CoV-2 depend on heparan sulfate proteoglycans, EMBO J. 40 (2021), e106765, https://doi.org/10.15252/embj.2020106765.
[38] C.J. Mycroft-West, et al., Heparin inhibits cellular invasion by SARS-CoV-2: structural dependence of the interaction of the spike S1 receptor-binding domain with heparin, Thromb. Haemost. 120 (2020) 1700–1715, https://doi.org/10.1055/s-0040-1721319.
[39] S.Y. Kim, et al., Characterization of heparin and severe acute respiratory syndrome-related coronavirus 2 (SARS-CoV-2) spike glycoprotein binding interactions, Antivir. Res. 181 (2020), 104873, https://doi.org/10.1016/j.antiviral.2020.104873.
[40] Y. Yang, D.G. Ivanov, I.A. Kaltashov, The challenge of structural heterogeneity in the native mass spectrometry studies of the SARS-CoV-2 spike protein interactions with its host cell-surface receptor, Anal. Bioanal. Chem. 413 (2021) 7205–7214, https://doi.org/10.1007/s00216-021-03601-3.
[41] T. Tang, M. Bidon, J.A. Jaimes, G.R. Whittaker, S. Daniel, Coronavirus membrane fusion mechanism offers a potential target for antiviral development, Antivir. Res. 178 (2020), 104792, https://doi.org/10.1016/j.antiviral.2020.104792.
[42] S. Belouzard, Mécanismes d'entrée des coronavirus, Virologie 14 (2010) 285–299.
[43] S. Xia, et al., The role of furin cleavage site in SARS-CoV-2 spike protein-mediated membrane fusion in the presence or absence of trypsin, Signal Transduct. Target. Ther. 5 (2020) 92, https://doi.org/10.1038/s41392-020-0184-0.
[44] N.C. Rockwell, D.J. Krysan, T. Komiyama, R.S. Fuller, Precursor processing by kex2/furin proteases, Chem. Rev. 102 (2002) 4525–4548, https://doi.org/10.1021/cr010168i.
[45] D.F. Steiner, The proprotein convertases, Curr. Opin. Chem. Biol. 2 (1998) 31–39, https://doi.org/10.1016/s1367-5931(98)80033-1.
[46] N.G. Seidah, A. Pasquato, U. Andréo, How do enveloped viruses exploit the secretory Proprotein convertases to regulate infectivity and spread? Viruses 13 (2021) https://doi.org/10.3390/v13071229.
[47] E. Braun, D. Sauter, Furin-mediated protein processing in infectious diseases and cancer, Clin. Transl. Immunol. 8 (2019), e1073, https://doi.org/10.1002/cti2.1073.
[48] V.M. Gordon, K.R. Klimpel, N. Arora, M.A. Henderson, S.H. Leppla, Proteolytic activation of bacterial toxins by eukaryotic cells is performed by furin and by additional cellular proteases, Infect. Immun. 63 (1995) 82–87.
[49] J.A. Young, R.J. Collier, Anthrax toxin: receptor binding, internalization, pore formation, and translocation, Annu. Rev. Biochem. 76 (2007) 243–265, https://doi.org/10.1146/annurev.biochem.75.103004.142728.
[50] E.R. Kastenhuber, et al., Coagulation factors directly cleave SARS-CoV-2 spike and enhance viral entry, bioRxiv (2021), https://doi.org/10.1101/2021.03.31.437960.
[51] Z. Obradovic, et al., Predicting intrinsic disorder from amino acid sequence, Proteins 53 (Suppl. 6) (2003) 566–572.
[52] D. Wrapp, et al., Cryo-EM structure of the 2019-nCoV spike in the prefusion conformation, Science (New York, *N.Y.)* 367 (2020) 1260–1263, https://doi.org/10.1126/science.abb2507.
[53] Y. Cai, et al., Distinct conformational states of SARS-CoV-2 spike protein, Science (New York, N.Y.) 369 (2020) 1586–1592, https://doi.org/10.1126/science.abd4251.
[54] A.F.M. Gavriilidou, K. Sokratous, H.Y. Yen, L. De Colibus, High-throughput native mass spectrometry screening in drug discovery, Front. Mol. Biosci. 9 (2022), 837901, https://doi.org/10.3389/fmolb.2022.837901.
[55] P. Gouzerh, M. Che, From Scheele and Berzelius to Muller - Polyoxometalates (POMs) revisited and the "missing link" between the bottom up and top down approaches, Actual. Chim. 9-22 (2006).
[56] A. Bijelic, M. Aureliano, A. Rompel, Polyoxometalates as potential next-generation Metallodrugs in the combat against Cancer, Angew. Chem. Int. Ed. Eng. 58 (2019) 2980–2999, https://doi.org/10.1002/anie.201803868.
[57] A. Bijelic, M. Aureliano, A. Rompel, The antibacterial activity of polyoxometalates: structures, antibiotic effects and future perspectives, Chem. Commun. 54 (2018) 1153–1169, https://doi.org/10.1039/C7CC07549A.
[58] S. Shigeta, S. Mori, T. Yamase, N. Yamamoto, N. Yamamoto, Anti-RNA virus activity of polyoxometalates, Biomed. Pharmacother. 60 (2006) 211–219, https://doi.org/10.1016/j.biopha.2006.03.009.
[59] S. Semiz, Vanadium as potential therapeutic agent for COVID-19: a focus on its antiviral, antiinflamatory, and antihyperglycemic effects, J. Trace Elem. Med. Biol. 69 (2022), 126887, https://doi.org/10.1016/j.jtemb.2021.126887.
[60] I. Navabshan, et al., Computational lock and Key and dynamic trajectory analysis of natural Biophors against COVID-19 spike protein to identify effective Lead molecules, Mol. Biotechnol. 63 (2021) 898–908, https://doi.org/10.1007/s12033-021-00358-z.
[61] C. Mycroft-West, et al., The 2019 coronavirus (SARS-CoV-2) surface protein (spike) S1 receptor binding domain undergoes conformational change upon heparin binding, bioRxiv (2020), https://doi.org/10.1101/2020.02.29.971093 %J bioRxiv doi: 10.1101/2020.02.29.971093.
[62] R. Tandon, et al., Effective Inhibition of SARS-CoV-2 Entry by Heparin and Enoxaparin Derivatives, bioRxiv (2020), https://doi.org/10.1101/2020.06.08.140236%J bioRxiv doi: 10.1101/2020.06.08.140236, 2020.2006.2008.140236.
[63] P. Prandoni, et al., The hazard of fondaparinux in non-critically ill patients with COVID-19: retrospective controlled study versus enoxaparin, Thromb. Res. 196 (2020) 395–397, https://doi.org/10.1016/j.thromres.2020.09.024.